High-Voltage Energy Harvesting and Storage System for Internet of Things Indoor Application

High-Voltage Energy Harvesting and Storage System for Internet of Things Indoor Application

Roberto Speranza, Pietro Zaccagnini, Adriano Sacco, and Andrea Lamberti**

On the path toward independence from fossil fuels, solar energy is the most promising solution, but it needs a robust and reliable storage system to face its intrinsic fluctuations due to location, day cycle, and weather. The integration between energy harvesting and storage (H&S) technologies is a must toward clean energy production, and it becomes even more appealing considering the possibility of producing electricity not only from direct sunlight but also from diffuse light and indoor illumination. Herein, a dye-sensitized solar module (DSSM) developed to harvest indoor illumination and directly store it into an electrical double-layer capacitor (EDLC) is presented. Five series-connected dye-sensitized solar cells are fabricated on the same substrate and the module is integrated with a high-voltage EDLC. The integrated device is characterized under indoor light sources such as light emitting diodes and fluorescent lamps. The results show one of the highest efficiencies ever reported for a high-voltage DSSM under indoor illumination (16.27%), the largest voltage window ever reported for an indoor H&S device based on DSSM and EDLC—up to 3 V—and an overall photoelectric conversion and storage efficiency of 9.73% under indoor illumination.

1. Introduction

The exponential growth of the population and the necessarily rapid industrial evolution has led to an ever-increasing energy demand, now no longer sustainable with nonrenewable energy sources (N-RES).[1] Indeed, N-RES represent the major actors in the environmental problems actually affecting our planet, conditioning human's life, ecosystems, buildings, materials resources, and the climate change.[2] Considering that a reliable estimation of these fossil sources does not go beyond the next 30 years, it is essential and absolutely necessary to move toward renewable energy sources.[3]

Moreover, also off-grid energy systems are becoming of paramount importance as the demands for continuous data processing and transmission for the Internet of Things (IoT), smart cities, and autonomous integrated devices grow.[4]

Among the possible available alternatives to traditional polluting sources, the solar one is the most promising solution.[5] Furthermore, many photovoltaic generations exist, from the first generation based on well-known mono- and polycrystalline silicon-based cells up to the third one that includes many kinds of technologies.[6] Among the third-generation devices, currently dye-sensitized solar cell (DSSC) has gained significant attention because of its advantages such as low production cost, long life, low light performance, variety, and mechanical robustness.[7] Moreover, DSSC showed an impressive light-to-energy conversion efficiency when employed under low-light illumination, diffuse solar radiation, and indoor light sources.[8] Additionally, low-temperature- and atmospheric-pressure-based manufacturing processes make them compatible with roll-to-roll fabrication. This makes DSSC an engaging alternative in the landscape of recovering energy from indoor illumination and directly power low-consuming devices (e.g., IoT devices).[9]

One of the main issues strictly related to the photovoltaics relies on the energy storage. Indeed, the intrinsic fluctuations of solar light due to location, day cycle, and weather make it necessary to connect with storage systems. The integration between energy harvesting and storage (H&S) technologies is a must toward clean energy production and it becomes even more appealing considering the possibility of producing electricity not only from direct sunlight but also from diffuse light and indoor illumination.[10,11]

To the best of our knowledge, commercial technologies of plug-and-use light H&S technologies do not exist. The only examples where photovoltaic and storage devices are coupled are demonstrators presented by the companies fabricating the solar cells, the storage devices, or external power management electronic components (e.g., Epishine, Cap-XX, E-peas, Fujikura, Dracula Technologies).

In all these cases, additional external electronics is needed to match the solar cell output to the energy storage devices.[12] This "external" solar cell integration with rechargeable devices increases overall device footprint, ohmic transport losses, and may reduce overall performances due to the nonunitary efficiency of each discrete component.

R. Speranza, P. Zaccagnini, A. Lamberti
Politecnico di Torino
Department of Applied Science and Technology (DISAT)
10129 Torino, Italy
E-mail: roberto.speranza@iit.it; andrea.lamberti@polito.it

R. Speranza, P. Zaccagnini, A. Sacco, A. Lamberti
Center for Sustainable Future Technologies
Istituto Italiano di Tecnologia
10129, Torino, Italy

The ORCID identification number(s) for the author(s) of this article can be found under https://doi.org/10.1002/solr.202200245.

DOI: 10.1002/solr.202200245

More recently, a stricter integration was obtained by sharing the electrodes of the two systems. In this way, 3- and 2-terminal devices have been proposed with obvious advantage in terms of energy mismatch compensation, smaller volume, and lower weight.[13–17]

Regarding the storage section, electrochemical double-layer capacitors (EDLCs) represent a promising solution because they can sustain an incredible number of cycles without appreciably changing the capacitance nominal value and they are less sensitive to the output voltage of the harvesting section with respect to rechargeable batteries.[18] These features perfectly match with the intermittent character of photovoltaic energy conversion and in particular with the indoor and IoT applications cited above.[19]

Finally, in order to improve the output voltage and power of the whole integrated device, photovoltaic modules made by cells in series are required. There are only few reports showing the integration of dye-sensitized solar module (DSSM) and supercapacitors.[20,21] Scalia et al. demonstrate the possibility to fabricate a H&S device exploiting DSSM and ionic liquid-based supercapacitors.[21] Herein, we move further with respect to this previous study by increasing up to five DSSCs the module and by sharing the fluorine-doped tin oxide (FTO) current collector with the supercapacitor in order to achieve a 3-terminal device. The integrated H&S device was able to provide 3 V as a maximum output voltage when employed either under simulated solar light or under indoor artificial light, with an overall photoelectric conversion and storage efficiency of 1.61% and 9.73%, respectively.

2. Results and Discussion

The purpose of this work was to present a fully integrated portable H&S system for low-power indoor applications. The device represents an evolution of the one fabricated in our group and reported by Scalia et al. in 2018.[21] In Scalia's work, the harvester was a 4-cell DSSM able to provide a maximum output voltage of 2.57 V with a power conversion efficiency (PCE) of 2.25%. For the storage section, a 233 mF cm^{-2} EDLC was fabricated, and the two devices were stacked vertically and externally connected. For both devices, FTO-coated glass was used as the current collector. In this work, the fabrication procedure was upgraded to produce the H&S sections on the same shared current collector, achieving a higher level of integration and avoiding the need for external connections which often cause electrical losses. The completed device can be seen in **Figure 1**. Moreover, we show that the device can represent a promising solution for indoor low-power applications. To do this, first we characterized separately the DSSM and the EDLC and then the whole integrated H&S device, in different illumination conditions.

2.1. Characterization of the DSSM Under Different Illumination Conditions

The DSSM was characterized first under simulated solar illumination (AM1.5). The *I–V* and *P–V* curves are reported in **Figure 2**a. The main photovoltaic parameters, reported in **Table 1**, indicate a significant improvement in the overall performance of the DSSM with respect to the results reported by Scalia et al. As expected, the additional solar cell in the series connection led to a 27% relative increase in the open-circuit voltage. Interestingly enough, the short-circuit current density also increased by 19% with respect to the 4-cell DSSM reported by Scalia et al., when calculated with respect to the average single cell active area. This is significant because the transparent TiO_2 semiconducting paste used in this work for the photoanode fabrication, is reported to result in a lower photogenerated current when compared to its opaque counterpart used by Scalia et al.[21] The reason for the better performance could be related to the lower active area of the single DSSC in this work with

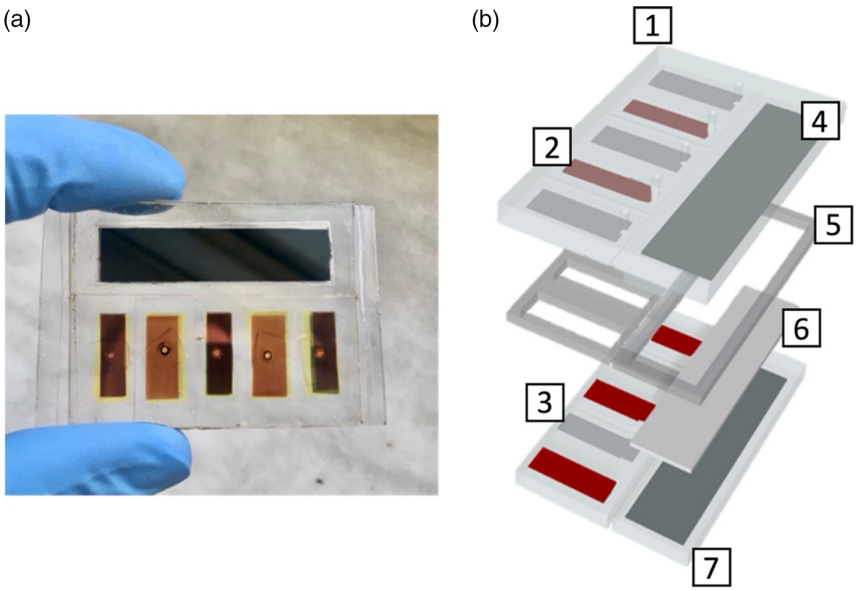

Figure 1. a) Photograph of the integrated device. b) 3D structure of the components of the device: 1) front shared current collector; 2) DSSC photoanode; 3) DSSC counter electrode; 4) SC active material; 5) thermoplastic sealant; 6) porous separator; and 7) back shared current collector.

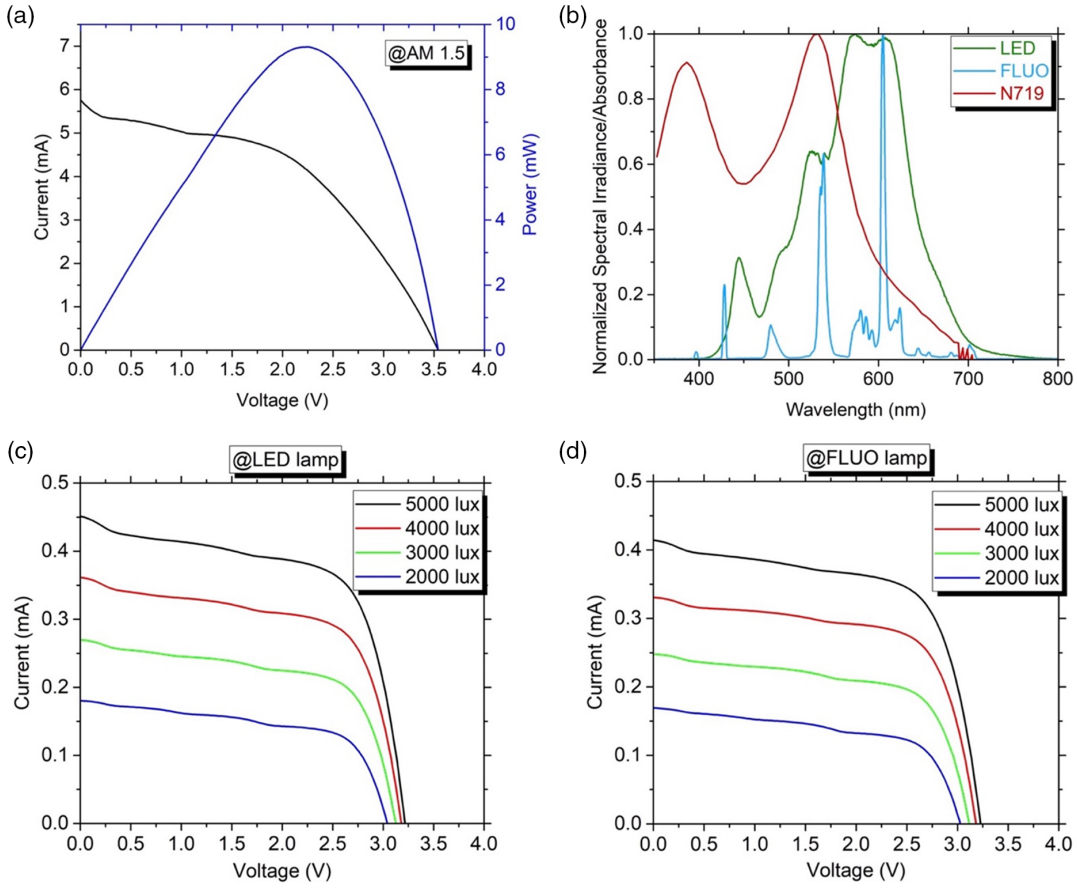

Figure 2. a) Current–voltage and power–voltage curves of the DSSM characterized under standard simulated AM1.5 solar spectrum. b) Normalized spectral irradiance of indoor LED and fluorescent lamp/ absorbance spectra of N719 dye. c) Current–voltage characteristic of the DSSC under indoor fluorescent lamp. d) Current–voltage characteristic of the DSSC under indoor LED lamp.

Table 1. Summary of the photovoltaic parameter of the DSSM at different illumination condition.

Light source	P_{in} [mW cm^{-2}]	Lux	I_{sc} [mA]	V_{oc} [V]	P_{max} [mW]	FF	Efficiency [%]
AM1.5	100		5.76	3.54	9.31	0.46	2.77
LED	1.7	5000	0.451	3.22	0.926	0.64	16.27
	1.4	4000	0.362	3.18	0.735	0.64	15.66
	1.0	3000	0.270	3.13	0.532	0.63	15.84
	0.7	2000	0.181	3.04	0.334	0.61	14.27
FLUO	1.6	5000	0.415	3.23	0.871	0.65	16.20
	1.3	4000	0.331	3.18	0.695	0.66	15.9
	0.9	3000	0.248	3.12	0.493	0.64	16.37
	0.6	2000	0.169	3.03	0.307	0.60	15.24

respect to Scalia's. Previous studies reported that lower active areas lead to an enhancement in the photocurrent generation due to an increased electron lifetime and reduced electron–hole recombination.[22–24] These improvements led to a PCE for the DSSM of 2.77%.

A known drawback of series-connected solar cells is the possible mismatch in the current photogenerated by each element of the series. This leads to a step-like *I–V* characteristic where each plateau is related to a different current photogenerated by the single solar cells.[25] To limit this problem, the active area of the front-illuminated cells was lower than the one of the back-illuminated cells, with a ratio of 1.44.

To investigate the behavior of the DSSM when employed in an indoor environment, the solar module was also characterized under artificial illumination, with the setup described in the previous section. A low consuming fluorescent lamp (Megaman) and a low consuming LED lamp (SPL) were used. Their emission spectra are reported in Figure 2b and the absorbance spectrum of the N719 dye is reported for comparison. The *I–V* characteristics of the DSSM were recorded illuminating the device at different illuminance levels. The obtained curves are reported in Figure 2c,d. As expected, the photogenerated current evidently decreases when illuminated with the indoor lamps with respect to the simulated solar spectrum. This is due to the lower value of the incident power. Nevertheless, it can be observed that the power conversion efficiency significantly increases, with peak values of 16.27% and 16.20% when illuminated at 5000 lux with a LED and a fluorescent lamp, respectively. The reason for the

performance improvements is to be found in two main factors. First, at lower incident power, a lower number of photons reaches the active materials and so less electrons are photogenerated; if on one side this leads to a lower photogenerated current, on the other side it reduces the electron–hole recombination rate and so a higher portion of photogenerated electrons are extracted from the active material.[26] However, this is always true when DSSCs are irradiated with low illumination values, regardless of the light source. The second factor strictly related to indoor illumination is to be found in spectral matching. As it can be observed in Figure 2b, the absorbance spectrum of the N719 dye used in this work has an absorbance peak centered in the visible region of the light spectrum. This leads to an improved ability to absorb the photons emitted at wavelengths that falls in the visible part of the light spectrum, which is the case of the common modern sources of indoor illumination. These results are in line to the findings reported in other works and confirm that DSSCs are a promising technology for indoor and low light applications.[8,10,27]

2.2. Characterization of EDLC

The performances of the EDLC were first characterized by performing a cyclic voltammetry (CV) at different scan rates, ranging from 1 to 50 mV s^{-1} and an electrochemical impedance spectroscopy. The results are reported in **Figure 3**a,b. The ideal rectangular behavior, expected from the CV, results slightly deformed with a resistive component possibly connected to the relatively high sheet resistance of the FTO current collector. This behavior, which becomes even more evident at faster scan rates, appears to confirm the results reported in other works where FTO-coated glass was used as current collector.[21] To further investigate the electrochemical behavior of the storage section of the device, a cyclic constant current charge–discharge test was performed at different current densities, ranging from 0.1 to 2 mA cm^{-2} (Figure 3c). The EDLC was charged applying a constant current up to a voltage of 3 V. As the maximum output voltage achievable from the DSSM was 3.54 V, equal to its V_{oc}, a maximum charging voltage of 3 V was chosen for the EDLC. In fact, a voltage closer to the V_{oc} of the DSSM could have led to photocharging currents too small, comparable to the self-discharging current of the EDLC, leading to a plateau in the photocharging process. The results show the characteristic triangular shape of EDLC from which a capacitance of 98 mF cm^{-2} can be calculated (at 0.3 mA cm^{-2}). In Figure S1, Supporting Information, the coulombic efficiency and the capacitance retention at different current density are reported. It can be observed that at higher current rates, the coulombic efficiency of the device increases while its capacitance reduces, which is in

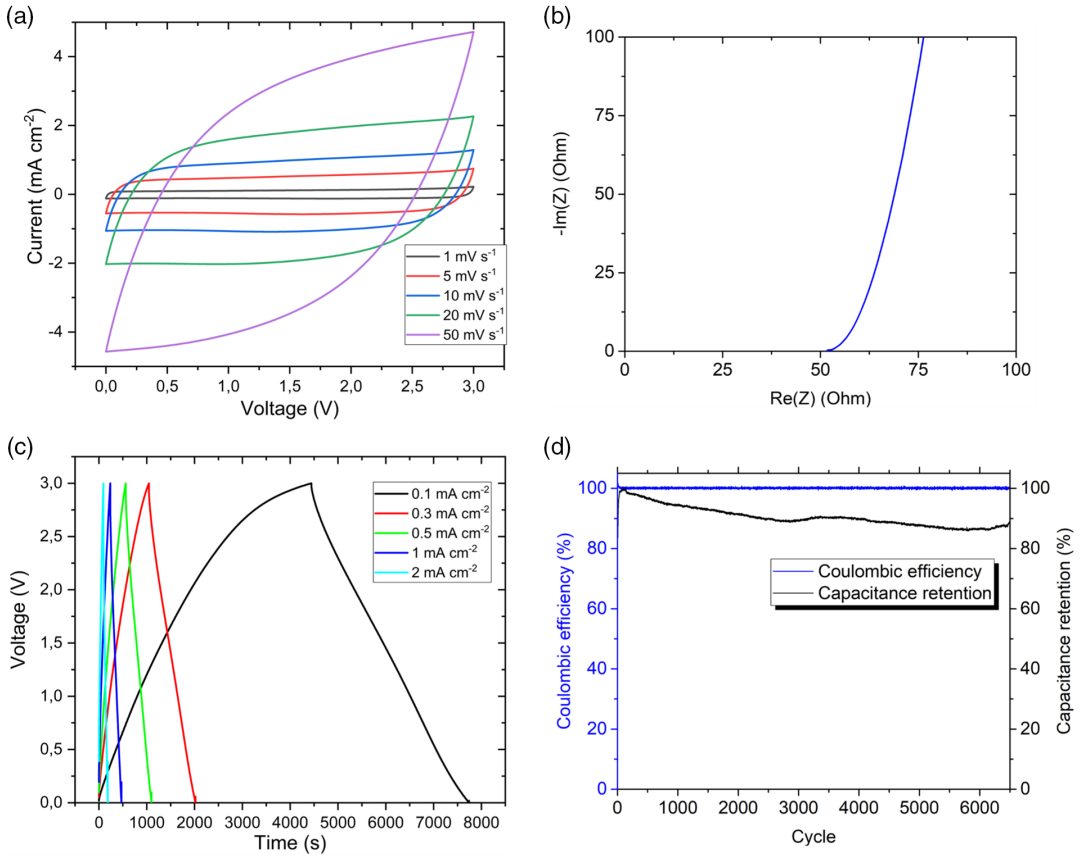

Figure 3. Electrochemical characterization of the supercapacitor. a) CV performed at 1, 5, 10, 20, and 50 mV s^{-1}; b) electrochemical impedance spectroscopy measurement (Nyquist plot) collected between 10 mHz and 1 MHz at; c) voltage profile during CCCD experiment recorded at 0.1, 0.3, 0.5, 1, and 2 mA cm^{-2}; d) cycling stability CCCD test performed at 0.37 mA cm^{-2} for 6000 cycles.

line with the results obtained from the CV. Here, the highly resistive FTO current collector limits the performance of the SC when it is employed in high current conditions. Nevertheless, performing a repeated galvanostatic charge–discharge test at 0.37 mA cm^{-2} for 6000 cycles, the stability of the SC was successfully asserted (Figure 3d). As expected, the device shows a very stable coulombic efficiency of around 99% over the whole measurement, and a promising capacitance retention with a value as high as 90% after 6000 charge–discharge cycles. These results show how the EDLC represents the best storage solution to stabilize the output of a solar module, being able to withstand the high number of charge and discharge cycles inevitably caused by the intermittent nature of photovoltaic power. However, in future developments, a strategy to reduce the resistance of the current collector should be considered.

2.3. Characterization of the Integrated H&S Device

Once the behavior of the two sections of the integrated H&S device was characterized, the goal is to show how it could represent a viable solution to harvest and directly store photovoltaic energy, both from solar light and from indoor illumination sources. For this purpose, a photocharge/discharge test was performed under different illumination conditions. The results are shown in **Figure 4**a,b. It can be observed that, when the device is illuminated under simulated solar spectrum, the EDLC is charged up to 3 V in 11.5 min. This high charging voltage is easily achieved before any saturation behavior is observed. This gives a first confirmation of the good matching between the power generation behavior of the DSSM and the storage ability of the EDLC: below the maximum charging voltage of 3 V, the DSSM is able to provide a current higher than 2 mA (Figure 2), which results to be enough to compensate any internal losses of the device (e.g., self-discharge of the EDLC, parasitic resistive effects), avoiding the appearance of a saturation plateau observed in other works reported in literature.[21,28] Moreover, the variation of the slope of the photocharging profile confirms that the DSSM is charging the EDLC with a nonconstant current, depending on the *I–V* characteristic of the solar module. It is clear, then, how the characteristic high power density of the EDLCs makes them one of the best technologies to be directly integrated with photovoltaic modules, differently from batteries that are known to be highly sensitive to the depth and velocity of charging.[29] After each photocharging step, the device was discharged at different constant current values, ranging from 1 mA (0.18 mA cm^{-2}) to 10 mA (1.8 mA cm^{-2}), as reported in Figure 4a. Here, the same discharging current selected by Scalia et al. was selected for comparison, with the difference that in our work, being the area of the capacitor more than three times smaller, the resulting discharging current densities are three times higher. Nevertheless, a discharge capacity of 0.095 mAh cm^{-2} was obtained at 1 mA discharge and 0.066 mAh cm^{-2} at 10 mA discharge, with a capacity retention of 69% when the discharging current was increase by one order of magnitude, which represents a further improvement with respect to the results reported by Scalia et al. Similar results are obtained when the device is illuminated by indoor light sources. Here, the charging time is inevitably longer, and the device reaches the goal voltage of 3 V after 91 and 101 min when illuminated with an LED and a fluorescent lamp, respectively. Nevertheless, the slope of the photocharging curve is more stable which is connected to the higher fill factor (FF) of the *I–V* characteristic of the DSSM under indoor illumination. Again, no saturation is observed which is relevant and indicates that the self-discharge current of the EDLC is still lower than the photocharging current of the DSSM under indoor illumination and close to the open-circuit voltage. When characterized under indoor light, the discharge capacity of the device reaches 0.101 mAh cm^{-2} when evaluated form a galvanostatic discharge at 1 mA (0.18 mA cm^{-2}) constant current. Here, the EDLC shows a maximum specific capacitance of 124.1 mF cm^{-2}, higher than the value evaluated from the GCD reported in the previous section and recorded at 0.37 mA cm^{-2}. This improvement is connected to the fact that under indoor illumination the current photogenerated by the DSSM decreases. Whether this leads to a longer charging time, the lower current allows a more uniform charging process of the EDLC. It is known that for porous electrodes, increasing the charging velocity leads to an incomplete charging if the charging time scale is lower than the time constant of the capacitive material.[30] To quantify the performance of the H&S device, the overall photoelectric conversion and storage efficiency (OPECSE) was calculated and reported with respect to the photocharge voltage and to the photocharging time in Figure 4c–f. When characterized under simulated solar spectrum, the devices reach a maximum overall efficiency of 1.61% at a maximum voltage of 2.19 V, equal to 73% of the maximum achievable voltage. This value is further increased when the device is characterized under indoor light: maximum overall efficiencies of 9.73% and 9.29% are achieved at maximum charging voltage of 2.85 and 2.8 V under LED and fluorescent lamp, respectively. Here, it is clear how the overall performance of the device increases when characterized under indoor illumination with respect to the simulated solar spectrum. It can be observed how in the indoor case, the overall efficiency increases almost linearly during the whole photocharging phase, reaching the maximum value at a voltage equal to 95% and 93.3% under LED and fluorescent lamp, respectively. This improvement is clearly connected to higher fill factor of the DSSM under indoor light and to the better exploitation of the total capacitance of the EDLC when charged at lower current rates. If the overall efficiency is reported with respect to the photocharging time (Figure 4d,f), it is clear how, in the case of the simulated solar spectrum, it increases quickly during the first minutes and then steadily decreases. Under indoor light illumination instead, the OPECSE increases during the whole photocharging time.

One of the main problems of this research sector is the lack of a standard for the comparison of the results obtained in the literature. Moreover, not all the works report the measurement conditions or make comparisons by fixing one of the main electrical parameters of interest. For this reason, we have decided to collect the main results of integrated devices including third-generation solar cells and energy storage devices (batteries and supercapacitors) in terms of OPECSE versus voltage window (**Figure 5**).[14,19,30–53] Among the collected works, the ones characterized under simulated solar spectrum have been reported in black while the ones characterized under indoor light were reported in red. Different symbols were used instead

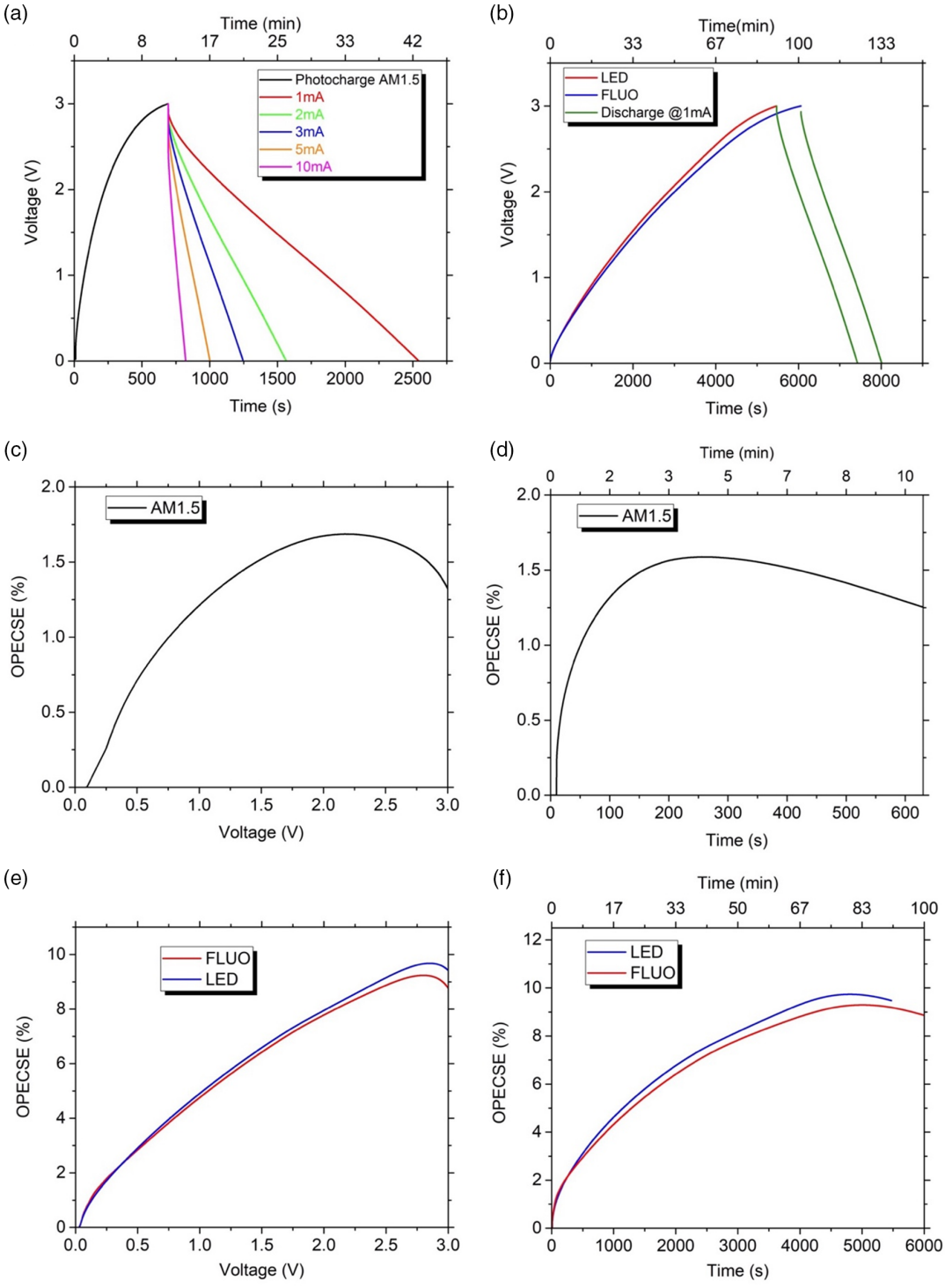

Figure 4. Performances of the integrated H&S device. a) Photocharge–discharge test performed under AM1.5 simulated solar spectrum and at different discharge currents; b) photocharge–discharge test performed under LED and fluorescent artificial light and at 1 mA discharge current; c,d) OPECSE with respect to charging voltage and to charging time under AM1.5 simulated solar spectrum; e,f) OPECSE with respect to charging voltage and to charging time under LED and fluorescent artificial light.

to identify the photovoltaic and energy storage technologies employed. As it can be seen, this work represents the integrated H&S device based on DSSM and an EDLC with the highest reported output voltage equal to 3 V and with the highest reported overall efficiency, equal to 9.73%. Moreover, it outperforms several integrated devices where perovskites solar cells

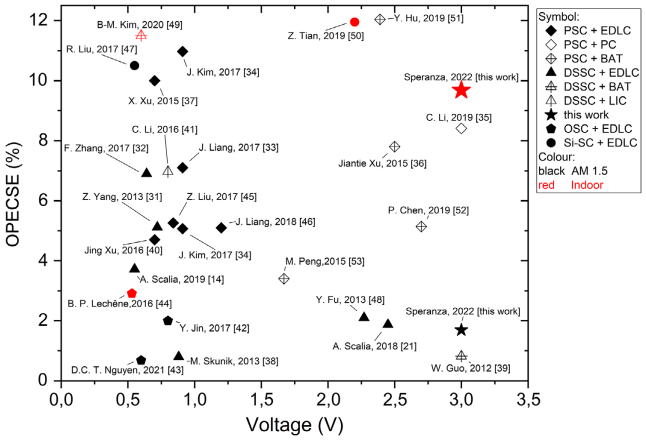

Figure 5. Overall H&S efficiency comparison with several works reported in the literature. DSSC, dye-sensitized solar cells; PSC, perovskite solar cells; OSC, organic solar cells; Si-SC, silicon solar cells; EDLC, electrical double-layer capacitors; PC, pseudocapacitors; BAT, battery; LIC, lithium-ion capacitors.

were employed as harvesters and batteries were employed as energy storage, showing also the highest overall efficiency for a 3 V integrated device, independently from the employed H&S technologies.

3. Conclusion

In this article, we report an integrated energy H&S system optimized for indoor applications, composed of five DSSCs and an electrochemical capacitor fabricated on a shared current collector. The DSSM and the SC were assembled on the same conductive glass current collector to achieve a higher level of integration with respect to similar devices reported before. DSSCs were selected as the energy harvesters thanks to their high efficiency under artificial light illumination conditions while an ionic liquid-based electrochemical capacitor was selected as the storage section because it was able to withstand the output voltage provided by the DSSM and the high output power variability of the solar module at different illumination condition. The device showed the highest output voltage of 3 V and the highest overall energy conversion and storage efficiency, equal to 9.73%, ever reported for an integrated device with these technologies. We characterized the harvesting section of the device under simulated standard solar spectrum and under artificial light illumination condition obtaining a photovoltaic efficiency of 2.77% and 16.27%, respectively. We also characterized the electrochemical capacitor showing a high stability within the desired high-voltage window of 3 V and a high cyclability with a coulombic efficiency of 99% and a capacitance retention of 90% after 6000 charge–discharge cycles and a maximum specific capacitance of 124.1 mF cm^{-2}. The integrated H&S device was characterized under simulated solar spectrum and under artificial light illumination showing a maximum overall photoelectric conversion and storage efficiency of 1.61% and 9.73%, respectively, showing a maximum discharge capacity of 0.54 mAh (0.1 mAh cm^{-2}). The outstanding efficiency showed by the integrated device under artificial illumination conditions makes these systems highly compatible with application where ambient light can be harvested and directly stored to power low consuming devices such as IoT sensors.

4. Experimental Section

Materials: FTO-coated glass (15 Ω sq^{-1}), thermoplastic sealing film (60 µm, Meltonix), and Ruthenizer 535-bisTBA (N719, dye) were purchased from Solaronix. Transparent nanoparticle TiO_2 paste was purchased from Dyesol (18NR-T). Sodium iodide (NaI) and iodine (I_2) were purchased from Sigma-Aldrich, while methoxypropionitrile (MPN) (CH_3OCH_2-CH_2CN) and 4-*tert*-butylpyridine (TBP) were purchased from Merck. Activated carbon (AC) YP-50 F powder was provided by Kuraray. Carbon black (CB) C65 powder was provided from Imerys. Sodium carboxymethyl cellulose (CMC) was purchased from MTI. Cellgard 3501 polypropylene–polyethylene–polypropylene (PP/PE/PP) separator was provided by Cellgard. [EMIM][TFSI] (99.9%) ionic liquid was purchased from Solvionic.

Device Fabrication: The integration of the DSSM and the EDLC was carried out following an adapted version of the fabrication procedure reported by Scalia et al.[21] First, one 4 cm × 6 cm and two 2 cm × 6 cm plates of FTO glass were cut for the back and front electrodes of the device, respectively. The FTO layer of the back and one of the two front substrates were carefully scribed using a diamond tip, to form the W-type series connection of the DSSC.[54] Then five inlet holes (1 mm diameter) were drilled with a diamond tip through the back substrate for electrolyte filling. Subsequently, the glasses were accurately cleaned in ultrasonic bath (50% acetone, 50% ethanol) for 10 min, rinsed with ethanol, and then placed for 10 min on a hot plate at 100 °C to ensure complete solvent evaporation. An adhesive tape (80 µm thick) was used as masking layer for the TiO_2 paste deposition. Two 1.4 cm × 0.6 cm rectangular gaskets and three 1.4 cm × 0.4 cm rectangular gaskets were cut from the tape for the back and front substrate, respectively. The tape was placed on the glass plates and then a layer of TiO_2 paste was deposited via doctor blade technique. After removing the tape, the plates were placed on a hot plate at 90 °C to ensure solvent evaporation. Then, the plates were sintered at 500 °C for 30 min to electrically interconnect the TiO_2 nanoparticles and remove all binders and solvents residue. On the counter electrode regions, Pt films were sputtered with a thickness of 3 and 10 nm for the front and back substrates, respectively. At this stage, instead of soaking the plates in the sensitizing dye solution, as reported by Scalia et al, it was decided to carry out the EDLC fabrication because it requires some high-temperature stages that would be detrimental for the N719 dye. Therefore, a water-based slurry was prepared with a composition of 85 wt% AC, 10 wt% CB, and 5 wt% CMC. First, the CMC binder was dissolved at 80 °C in continuously stirred ultrapure (milliQ) H_2O with the appropriate ratio. Then, in the same condition, first CB and then AC were slowly added. Then, the slurry was left stirring overnight, in a closed container, at 80 °C to ensure homogeneous dissolution of all components. The adhesive tape was again placed on the front and back glass plates, two 1 cm × 5.4 cm rectangular gaskets were cut, and the prepared slurry was deposited via doctor blade technique. Then, the EDLC electrodes were dried first at room temperature in a fume hood for 5 h and then in a glass hoven under vacuum at 120 °C for 12 h. Finally, the EDLC was assembled in a dry room: a 1 cm × 5.4 cm rectangular PP/PE/PP separator was placed between the electrodes and wet with few drops of electrolyte. [EMIM][TFSI], thanks to its high electrochemical stability window, was selected as an electrolyte to withstand the high-voltage window intended for the H&S device. The device was sealed with two 60 µm thermoplastic films using a hot press at 110 °C. Once the EDLC was completed, the plates were soaked for 24 h in 0.3 mM N719 solution in ethanol to sensitize the DSSCs photoanodes. After rinsing with ethanol to remove any residual dye particles, the plates were dried under gentle nitrogen flow and then sealed with one 60 µm thermoplastic film using a hot press at 110 °C. Finally, the DSSCs were filled with electrolyte via vacuum

backfilling and the inlets were sealed using thermoplastic and small glass caps. The electrolyte for the DSSCs was prepared with the following composition: 0.45 M NaI, 0.056 M I_2, and 0.55 M 4-*tert*-butylpyridine dissolved in MPN.

DSSM Characterization: To test the DSSM performance under different illumination conditions, the device was characterized both under AM1.5 G spectrum using a Newport 91195 A solar simulator and under indoor light sources using a low consuming fluorescent lamp (12 V DC, 15 W, 2700 K, 800 lm from Megaman) and a low consuming LED lamp (12–60 V AC/DC, 10 W, 3000 K, 810 lm from SPL). The current–voltage (*I*–*V*) characteristics of the DSSM under different illumination conditions were measured using a Keithley 2440 source measure unit. The spectral irradiances of the indoor lamps were collected using a StellarNet EPP2000-UVN spectrometer while the illuminance and the incident power was measured using a Delta Ohm HD 2102.2 photo/radiometer. In the attempt to characterize the device under reproducible and steady conditions, a dedicated setup to simulate an indoor ambient was employed. The setup was identical to the one reported by Sacco et al.[27] and consisted of a wooden box with dimensions 70 cm × 40 cm × 40 cm. To simulate the effect of radiation-diffusing walls, the interior of the box was coated by a commercially available white, water paint for inside use, antitranspiring, and antistatic (Sikkens Alpha Isolux SF). The lamps were placed in one of the upper corners of the box and the DSSM was placed on the bottom of the box achieving a distance between the light source and the device of around 30 cm. From the measurements, the photoelectric conversion efficiency η of the DSSM was calculated according to the equation

$$\eta = \frac{V_{oc} \times J_{sc} \times FF}{G} \tag{1}$$

where V_{oc} is the open-circuit voltage, J_{sc} is the short-circuit current, FF is the fill factor, and G is the incident radiation power density.

EDLC Characterization: The EDLC performance was initially tested using a BioLogic VMP3 potentiostat. CV and an electrochemical impedance spectroscopy (EIS) were performed. Then, a more insightful characterization was conducted with an Arbin BT 2000 potentiostat and galvanostatic charge–discharge (GCD) measurements were performed from which the specific capacitance C_s, the coulombic efficiency (CE), and the capacitance retention (CR) of the EDLC were calculated. The specific capacitance C_s was calculated according to the equation

$$C_s = \frac{i_{dc}}{s \times A} \tag{2}$$

where i_{dc} is the galvanostatic discharge current, s is the slope of the linear discharge voltage, and A is the surface area of the EDLC.

H&S Characterization: The integrated device was characterized performing a photocharge/constant-current discharge test both under simulated AM1.5 G spectrum and under indoor light sources (fluorescent tube and LED lamp) and the measurements were performed using a Keithley 2440 source measure unit. During the photocharge step, the DSSM and the EDLC were connected in parallel, the device was exposed to the light source, and the voltage across the EDLC was measured. Immediately after, the DSSM was disconnected and the EDLC was discharged at a constant current value, measuring its voltage. From the measurement, the overall photoelectric conversion and storage efficiency (OPECSE) was calculated according to the equation

$$\text{OPECSE} = \frac{\frac{1}{2} \times C \times \Delta V^2}{G \times t \times S} \tag{3}$$

where C is the capacitance of the EDLC, ΔV is the difference between EDLC voltage and its open-circuit voltage, G is the incident radiation power density, t is the photocharging time, and S is the total active surface of the DSSM.

Supporting Information

Supporting Information is available from the Wiley Online Library or from the author.

Acknowledgements

Open Access Funding provided by Politecnico di Torino within the CRUI-CARE Agreement.

Conflict of Interest

The authors declare no conflict of interest.

Data Availability Statement

Research data are not shared.

Keywords

dye-sensitized solar cells, energy harvesting and storage, indoor energy harvesting, integrated devices, photosupercapacitors, portable devices

Received: March 18, 2022
Revised: May 25, 2022
Published online:

[1] L. Miller, R. Carriveau, *Sustain. Energy Technol. Assess.* **2019**, *35*, 172.
[2] S. Ali, S. Anwar, S. Nasreen, *Forman J. Econ. Stud.* **2017**, *00*, 177.
[3] T. Güney, *Int. J. Sustain. Dev. World Ecol.* **2019**, *26*, 389.
[4] C. Shen, S. Xu, Y. Xie, M. Sanghadasa, X. Wang, L. Lin, *J. Microelectromech. Syst.* **2017**, *26*, 949.
[5] N. Kannan, D. Vakeesan, *Renew. Sustain. Energy Rev.* **2016**, *62*, 1092.
[6] W. C. Sinke, *Renew. Energy* **2019**, *138*, 911.
[7] T. V. Arjunan, T. S. Senthil, *Mater. Technol.* **2013**, *28*, 9.
[8] D. Devadiga, M. Selvakumar, P. Shetty, M. S. Santosh, *J. Elec. Mater.* **2021**, *50*, 3187.
[9] A. Aslam, U. Mehmood, M. H. Arshad, A. Ishfaq, J. Zaheer, A. Ul Haq Khan, M. Sufyan, *Sol. Energy* **2020**, *207*, 874.
[10] G. Gokul, S. C. Pradhan, S. Soman, in *Advances In Solar Energy Research* (Eds.: H. Tyagi, A.K. Agarwal, P.R. Chakraborty, S. Powar), Springer Singapore, Singapore **2019**, pp. 281–316.
[11] A. Scalia, F. Bella, A. Lamberti, S. Bianco, C. Gerbaldi, E. Tresso, C. F. Pirri, *J. Power Sources* **2017**, *359*, 311.
[12] F. Yuan, Q. T. Zhang, S. Jin, H. Zhu, *IEEE Trans. Wirel. Commun.* **2015**, *14*, 698.
[13] Q. Zeng, Y. Lai, L. Jiang, F. Liu, X. Hao, L. Wang, M. A. Green, *Adv. Mater.* **2020**, *10*, 1903930.
[14] A. Scalia, F. Bella, A. Lamberti, C. Gerbaldi, E. Tresso, *Energy* **2019**, *166*, 789.
[15] Y. Wu, C. Li, Z. Tian, J. Sun, *J. Power Sources* **2020**, *478*, 228762.
[16] Y. Sun, X. Yan, *Sol. RRL* **2017**, *1*, 1700002.
[17] Y. Sun, P. Ma, L. Liu, J. Chen, X. Zhang, J. Lang, X. Yan, *Sol. RRL* **2018**, *2*, 1800223.
[18] W. Raza, F. Ali, N. Raza, Y. Luo, K.-H. Kim, J. Yang, S. Kumar, A. Mehmood, E. E. Kwon, *Nano Energy* **2018**, *52*, 441.
[19] C. Lethien, J. Le Bideau, T. Brousse, *Energy Environ. Sci.* **2019**, *12*, 96.
[20] A. Scalia, A. Varzi, A. Lamberti, T. Jacob, S. Passerini, *Front. Chem.* **2018**, *6*, 1.

[21] A. Scalia, A. Varzi, A. Lamberti, E. Tresso, S. Jeong, T. Jacob, S. Passerini, *Sustain. Energy Fuels* **2018**, *2*, 968.
[22] V. K. Vendra, J. Absher, S. R. Ellis, D. A. Amos, T. Druffel, M. K. Sunkara, *J. Electrochem. Soc.* **2012**, *159*, H728.
[23] A. Fakharuddin, P. S. Archana, Z. Kalidin, M. M. Yusoff, R. Jose, *RSC Adv.* **2013**, *3*, 2683.
[24] A. Mashreghi, F. Bahrami Moghadam, *J. Solid State Electrochem.* **2016**, *20*, 1361.
[25] S. Iwata, S. Ichiro Shibakawa, N. Imawaka, K. Yoshino, *Energy Rep.* **2018**, *4*, 8.
[26] M. Aftabuzzaman, S. Sarker, C. Lu, H. K. Kim, *J. Mater. Chem. A* **2021**, *9*, 24830.
[27] A. Sacco, L. Rolle, L. Scaltrito, E. Tresso, C. F. Pirri, *Appl. Energy* **2013**, *102*, 1295.
[28] C.-T. Chien, P. Hiralal, D.-Y. Wang, I.-S. Huang, C.-C. Chen, C.-W. Chen, G. A. J. Amaratunga, *Small* **2015**, *11*, 2929.
[29] V. Vega-Garita, L. Ramirez-Elizondo, N. Narayan, P. Bauer, *Progr. Photovolt. Res. Appl.* **2019**, *27*, 346.
[30] B. E. Conway, in *Electrochemical Supercapacitors*, Springer US, Boston, MA **1999**.
[31] Z. Yang, L. Li, Y. Luo, R. He, L. Qiu, H. Lin, H. Peng, *J. Mater. Chem. A* **2013**, *1*, 954.
[32] F. Zhang, W. Li, Z. Xu, M. Ye, W. Guo, H. Xu, X. Liu, *RSC Adv.* **2017**, *7*, 52988.
[33] J. Liang, G. Zhu, Z. Lu, P. Zhao, C. Wang, Y. Ma, Z. Xu, Y. Wang, Y. Hu, L. Ma, T. Chen, Z. Tie, J. Liu, Z. Jin, *J. Mater. Chem. A* **2018**, *6*, 2047.
[34] J. Kim, S. M. Lee, Y.-H. Hwang, S. Lee, B. Park, J.-H. Jang, K. Lee, *J. Mater. Chem. A* **2017**, *5*, 1906.
[35] C. Li, S. Cong, Z. Tian, Y. Song, L. Yu, C. Lu, Y. Shao, J. Li, G. Zou, M. H. Rümmeli, S. Dou, J. Sun, Z. Liu, *Nano Energy* **2019**, *60*, 247.
[36] J. Xu, Y. Chen, L. Dai, *Nat. Commun.* **2015**, *6*, 8103.
[37] X. Xu, S. Li, H. Zhang, Y. Shen, S. M. Zakeeruddin, M. Graetzel, Y.-B. Cheng, M. Wang, *ACS Nano* **2015**, *9*, 1782.
[38] M. Skunik-Nuckowska, K. Grzejszczyk, P. J. Kulesza, L. Yang, N. Vlachopoulos, L. Häggman, E. Johansson, A. Hagfeldt, *J. Power Sources* **2013**, *234*, 91.
[39] W. Guo, X. Xue, S. Wang, C. Lin, Z. L. Wang, *Nano Lett.* **2012**, *12*, 2520.
[40] J. Xu, Z. Ku, Y. Zhang, D. Chao, H. J. Fan, *Adv. Mater. Technol.* **2016**, *1*, 1600074.
[41] C. Li, Md. M. Islam, J. Moore, J. Sleppy, C. Morrison, K. Konstantinov, S. X. Dou, C. Renduchintala, J. Thomas, *Nat. Commun.* **2016**, *7*, 13319.
[42] Y. Jin, Z. Li, L. Qin, X. Liu, L. Mao, Y. Wang, F. Qin, Y. Liu, Y. Zhou, F. Zhang, *Adv. Mater. Interfaces* **2017**, *4*, 1700704.
[43] D. C. T. Nguyen, J. Shin, S.-K. Kim, S.-H. Lee, *ACS Appl. Energy Mater.* **2021**, *4*, 14014.
[44] B. P. Lechêne, M. Cowell, A. Pierre, J. W. Evans, P. K. Wright, A. C. Arias, *Nano Energy* **2016**, *26*, 631.
[45] Z. Liu, Y. Zhong, B. Sun, X. Liu, J. Han, T. Shi, Z. Tang, G. Liao, *ACS Appl. Mater. Interfaces* **2017**, *9*, 22361.
[46] J. Liang, G. Zhu, C. Wang, P. Zhao, Y. Wang, Y. Hu, L. Ma, Z. Tie, J. Liu, Z. Jin, *Nano Energy* **2018**, *52*, 239.
[47] R. Liu, J. Wang, T. Sun, M. Wang, C. Wu, H. Zou, T. Song, X. Zhang, S.-T. Lee, Z. L. Wang, B. Sun, *Nano Lett.* **2017**, *17*, 4240.
[48] Y. Fu, H. Wu, S. Ye, X. Cai, X. Yu, S. Hou, H. Kafafy, D. Zou, *Energy Environ. Sci.* **2013**, *6*, 805.
[49] B.-M. Kim, M.-H. Lee, V. S. Dilimon, J. S. Kim, J. S. Nam, Y.-G. Cho, H. K. Noh, D.-H. Roh, T.-H. Kwon, H.-K. Song, *Energy Environ. Sci.* **2020**, *13*, 1473.
[50] Z. Tian, X. Tong, G. Sheng, Y. Shao, L. Yu, V. Tung, J. Sun, R. B. Kaner, Z. Liu, *Nat. Commun.* **2019**, *10*, 4913.
[51] Y. Hu, Y. Bai, B. Luo, S. Wang, H. Hu, P. Chen, M. Lyu, J. Shapter, A. Rowan, L. Wang, *Adv. Mater.* **2019**, *9*, 1900872.
[52] P. Chen, G. Li, T. Li, X. Gao, *Adv. Sci.* **2019**, *6*, 1900620.
[53] M. Peng, K. Yan, H. Hu, D. Shen, W. Song, D. Zou, *J. Mater. Chem. C* **2015**, *3*, 2157.
[54] F. Giordano, E. Petrolati, T. M. Brown, A. Reale, A. Di Carlo, *IEEE Trans. Electron Dev.* **2011**, *58*, 2759.